arXiv:1612.04568v1 [cs.SY] 14 Dec 2016

Initial estimates for Wiener-Hammerstein models using phase-coupled multisines ⋆

Koen Tiels [a], Maarten Schoukens [a], Johan Schoukens [a]

[a] *Department ELEC, Vrije Universiteit Brussel, 1050 Brussels, Belgium*

Abstract

Block-oriented models are often used to model nonlinear systems. These models consist of linear dynamic (L) and nonlinear static (N) sub-blocks. This paper addresses the generation of initial estimates for a Wiener-Hammerstein model (LNL cascade). While it is easy to measure the product of the two linear blocks using a Gaussian excitation and linear identification methods, it is difficult to split the global dynamics over the individual blocks. This paper first proposes a well-designed multisine excitation with pairwise coupled random phases. Next, a modified best linear approximation is estimated on a shifted frequency grid. It is shown that this procedure creates a shift of the input dynamics with a known frequency offset, while the output dynamics do not shift. The resulting transfer function, which has complex coefficients due to the frequency shift, is estimated with a modified frequency domain estimation method. The identified poles and zeros can be assigned to either the input or output dynamics. Once this is done, it is shown in the literature that the remaining initialization problem can be solved much easier than the original one. The method is illustrated on experimental data obtained from the Wiener-Hammerstein benchmark system.

Key words: Block-oriented nonlinear system; Dynamic systems; Nonlinear systems; Phase-coupled multisines; System identification; Wiener-Hammerstein model.

1 Introduction

Even if all physical dynamic systems behave nonlinearly to some extent, we often use linear models to describe them. If the nonlinear distortions get too large, a linear model is insufficient, and a nonlinear model is required.

One possibility is to use block-oriented models (Billings & Fakhouri, 1982; Giri & Bai, 2010), which combine linear dynamic (L) and nonlinear static (N), i.e. memoryless, blocks. Due to this highly structured nature, block-oriented models offer insight about the system to the user. This can be useful in e.g. fault detection, to detect in which part of the system a fault occurred, e.g. changing dynamics in only part of the model. Block-oriented models are preferred when there are localized nonlinearities in the system, thus leading to a sparse representation of the system in terms of interconnected blocks. Due to the separation between the dynamics and the nonlinearities, block-oriented models also allow for an easy discretization (i.e. the conversion from a continuous-time to a discrete-time representation). We refer the reader to Giri & Bai (2010) for an elaborated discussion. The simplest block-oriented models are the Wiener model (LN cascade) and the Hammerstein model (NL cascade). They can be generalized to a Wiener-Hammerstein model (LNL cascade, see Fig. 1). Applications of Wiener-Hammerstein models can mainly be found in biology (Korenberg & Hunter, 1986; Dewhirst, Simpson, Angarita, Allen & Newland, 2010; Bai, Cai, Dudley-Javorosk & Shields, 2009), but also in the modeling of RF power amplifiers (Isaksson, Wisell & Rönnow, 2006).

Several identification methods have been proposed to identify Wiener-Hammerstein systems. Early work can be found in Billings & Fakhouri (1982); Korenberg & Hunter (1986). The maximum likelihood estimate is formulated in Chen & Fassois (1992). Wiener-Hammerstein systems are modeled as the cascade of well-selected Hammerstein models in Wills & Ninness (2012). The recursive identification of error-in-variables Wiener-Hammerstein systems is considered in Mu & Chen (2014). Both Chen & Fassois (1992) and

⋆ The material in this paper was partially presented at the 19th IFAC World Congress, August 24–29, 2014, Cape Town, South Africa. Corresponding author K. Tiels. Tel. +32 2 6293665. Fax +32 2 6292850.

Email addresses: Koen.Tiels@vub.ac.be (Koen Tiels), Maarten.Schoukens@vub.ac.be (Maarten Schoukens), Johan.Schoukens@vub.ac.be (Johan Schoukens).

This paper is a post-print of a paper submitted to and accepted for publication in Automatica.

©2015. *This manuscript version is made available under the CC-BY-NC-ND 4.0 license*

https://creativecommons.org/licenses/by-nc-nd/4.0/.

The publisher's version of this paper is available under the DOI: http://dx.doi.org/10.1016/j.automatica.2015.07.020.

Wills & Ninness (2012) indicate the importance of good initial estimates, but not how to obtain them. Sjöberg & Schoukens (2012) indicates the importance of good initial estimates on an example. The optimization of the model parameters can either converge extremely slowly or get trapped in a local optimum, even if the correct number of poles and zeros is assigned to both the input and the output dynamics, leading to Wiener-Hammerstein models that only fit about as well as a linear model.

Some approaches obtain initial estimates by using specifically designed experiments. For example, Vandersteen, Rolain & Schoukens (1997) proposes a series of experiments with large and small signal multisines. Weiss, Evans & Rees (1998) uses only two experiments with paired multisines, but the approach requires the estimation of the Volterra kernels of the system. Crama & Schoukens (2005) proposes an iterative initialization scheme that only requires one experiment of a well-designed multisine excitation.

A major difficulty is the generation of good initial values for the two linear blocks $R(q)$ and $S(q)$ of the Wiener-Hammerstein system (see Fig. 1). An initial estimate for the static nonlinearity can be obtained using a simple linear regression if a basis function expansion, linear-in-the-parameters, for the nonlinearity is used, and if the dynamics are initialized. The poles and the zeros of both $R(q)$ and $S(q)$ can be obtained from the best linear approximation (BLA) (Pintelon & Schoukens, 2012) of the Wiener-Hammerstein system. To obtain initial estimates for $R(q)$ and $S(q)$, the poles and the zeros of the BLA should be split over the individual transfer functions $R(q)$ and $S(q)$. Several methods have been proposed to make this split. The brute-force method in Sjöberg, Lauwers & Schoukens (2012) scans all possible splits, leading to an exponential scanning problem. The advanced method in Sjöberg et al. (2012) uses a basis function expansion for the input dynamics and one for the inverse of the output dynamics. A scanning procedure over the basis functions is proposed as well. Compared to the brute-force method, the number of scans is lower, but the computational time can still be large. The approach in Westwick & Schoukens (2012) not only uses the BLA, but also the so-called quadratic BLA (QBLA), a higher-order BLA from the squared input to the output residual of the first-order BLA. By doing so, the number of possible splits is reduced significantly. Due to the higher-order nature of the QBLA, however, long measurements are needed to obtain an accurate estimate. The nonparametric separation method proposed in Schoukens, Pintelon & Rolain (2014b) avoids the pole/zero assignment problem completely, but also uses the QBLA.

The method proposed in Schoukens, Tiels & Schoukens (2014a) and further developed in this paper uses again the first-order BLA. Using a well-designed excitation signal, the poles and the zeros of the input dynamics $R(q)$ shift with a frequency offset that can be chosen by the user, while the poles and the zeros of the output dynamics $S(q)$ remain invariant. Long measurement times can be avoided, because no use is made of higher-order BLAs. This paper generalizes the basic ideas in Schoukens et al. (2014a) from cubic nonlinearities to polynomial nonlinearities. Moreover, experimental results on the Wiener-Hammerstein benchmark system (Schoukens, Suykens & Ljung, 2009) are reported.

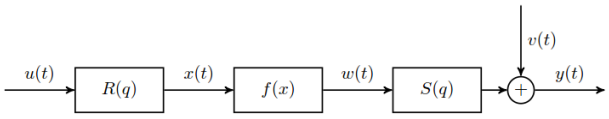

Fig. 1. A Wiener-Hammerstein system (R and S are linear dynamic systems and f is a nonlinear static system).

The rest of this paper is organized as follows. The basic setup is described in Section 2. A brief overview of the BLA is presented in Section 3. The proposed method is presented in Section 4. The experimental results on the Wiener-Hammerstein benchmark system are reported in Section 5. Finally, the conclusions are drawn in Section 6.

2 Setup

This section introduces some notation. It also presents the considered Wiener-Hammerstein system and the assumptions.

2.1 Notation

Without loss of generality, discrete-time systems are considered. Hence, the integer t denotes the time as a number of samples. The results in this paper generalize to continuous-time systems with some minor modifications.

Notation 1 ($X(k)$ and $x(t)$)**.** The discrete Fourier transform (DFT) of a time domain signal $x(t)$ is denoted by $X(k) = X(e^{j\omega_k})$, and is given by

$$X(k) = \frac{1}{\sqrt{N}} \sum_{t=0}^{N-1} x(t) e^{-j2\pi \frac{k}{N} t} . \tag{1}$$

The inverse DFT is given by

$$x(t) = \frac{1}{\sqrt{N}} \sum_{k=-N/2+1}^{N/2} X(k) e^{j2\pi \frac{k}{N} t} . \tag{2}$$

Notation 2 (q^{-1})**.** The backward shift operator is denoted by q^{-1}, i.e. $q^{-1}x(t) = x(t-1)$.

Notation 3 ($O(\cdot)$)**.** The notation h is an $O(N^\alpha)$ indicates that for N big enough, $|h(N)| \leq cN^\alpha$, where c is a strictly positive real number.

Notation 4 ($(\cdot)^*$)**.** The complex conjugate of a complex number X is denoted by X^*.

2.2 The Wiener-Hammerstein system

Consider the Wiener-Hammerstein system in Fig. 1, given by

$$\begin{aligned} x(t) &= R(q)u(t)\,, \\ w(t) &= f(x(t))\,, \\ y(t) &= S(q)w(t) + v(t)\,, \end{aligned} \tag{3}$$

where $R(q)$ and $S(q)$ are linear time-invariant (LTI) discrete-time transfer functions, i.e.

$$\begin{aligned} R(q) &= \frac{B_R(q)}{A_R(q)} = \frac{\sum_{l=0}^{n_R} b_{R,l} q^{-l}}{\sum_{l=0}^{m_R} a_{R,l} q^{-l}}\,, \\ S(q) &= \frac{B_S(q)}{A_S(q)} = \frac{\sum_{l=0}^{n_S} b_{S,l} q^{-l}}{\sum_{l=0}^{m_S} a_{S,l} q^{-l}}\,, \end{aligned} \tag{4}$$

and where $f(x)$ is a static nonlinear function. Only the input $u(t)$ and the noise-corrupted output $y(t)$ are available for measurement.

2.3 Assumptions

This paper addresses the generation of initial estimates for the linear dynamics $R(q)$ and $S(q)$. To do this, assumptions (A1)–(A4) are made.

(A1) The static nonlinearity $f(x)$ can be arbitrarily well approximated by a polynomial in the interval $[\min(x(t)), \max(x(t))]$. Hence, $f(x)$ can be thought of as $f(x) = \sum_{D=0}^{\infty} \gamma_D x^D$.

Note that a uniformly convergent polynomial approximation of a continuous nonlinearity is always possible on a closed interval due to the Weierstrass approximation theorem (Weisstein, n.d.). The type of convergence can be relaxed to mean-square convergence, thus allowing for some discontinuous nonlinearities as well.

(A2) At least one nonlinear odd term is present, i.e. there exists an odd $D \geq 3$ for which $\gamma_D \neq 0$.

Assumption (A2) is slightly stricter than the assumption of non-evenness of the nonlinearity, which is typically made in other BLA approaches. When facing an even nonlinearity, a slight DC offset is typically added to the input, such that the nonlinearity is no longer even around the new set-point. If the nonlinearity only has polynomial terms up to second degree, i.e. it is a parabola, then adding a DC offset to the input can make the nonlinearity non-even, but it will not create a nonlinear odd term.

(A3) The additive output noise $v(t)$ is a sequence of zero-mean filtered white noise that is independent of the excitation signal $u(t)$.

Under this assumption, the classical least-squares framework is known to result in consistent estimates of the BLA (Pintelon & Schoukens, 2012). To simplify the notation, and without loss of generality, the results in this paper are presented in the noise-free case. Input and process noise are not considered here. In general, this would result in biased estimates. A more involved errors-in-variables approach (e.g. Mu & Chen (2014)) is required to obtain unbiased estimates in this more general case.

(A4) The system operates in steady-state.

3 The BLA of a Wiener-Hammerstein system using random-phase multisines

This section briefly reviews the BLA of a system. Explicit expressions for the output spectrum of the BLA of a Wiener-Hammerstein system, excited by a random-phase multisine, are provided. These expressions will be convenient to set the ideas for the proposed method in Section 4, where phase-coupled multisines are proposed.

3.1 Random-phase multisine excitation

This paper considers multisine excitations.

Definition 1 (multisine)**.** A signal $u(t)$ is a multisine if

$$u(t) = \sum_{k=-N/2+1}^{N/2} U_k e^{j2\pi \frac{k}{N} t} \quad \text{for } t = 0, 1, \ldots, N-1\,, \tag{5}$$

where the Fourier coefficients $U_k = U_{-k}^* = |U_k| e^{j\phi_k}$ are either zero (no excitation present at frequency line k) or have a normalized amplitude $|U_k| = \frac{1}{\sqrt{N}} \check{U}\left(\frac{k}{N}\right)$, where $\check{U}\left(\frac{\omega}{2\pi}\right) \in \mathbb{R}^+$ is a uniformly bounded function.

Definition 2 (random-phase multisine)**.** A signal $u(t)$ is a random-phase multisine if it is a multisine (see Definition 1) where the phases ϕ_k are independently and identically distributed with the property $E\left\{e^{j\phi_k}\right\} = 0$.

3.2 The best linear approximation

The BLA of a system is defined as the linear system whose output approximates the system's output best in mean-square sense around the operating point (Pintelon & Schoukens, 2012), i.e.

Definition 3 (best linear approximation)**.**

$$G_{\mathrm{BLA}}(k) := \arg\min_{G(k)} E_u \left\{ \|\tilde{Y}(k) - G(k)\tilde{U}(k)\|^2 \right\}\,, \tag{6}$$

with

$$\begin{cases} \tilde{u}(t) = u(t) - E\{u(t)\} \\ \tilde{y}(t) = y(t) - E\{y(t)\} \end{cases}, \tag{7}$$

where G_{BLA} is the frequency response function (FRF) of the BLA, and where the expectation in (6) is taken with respect to the random input u.

Remark 1. In the remainder of this paper, it is assumed that the mean values are removed from the signals when a BLA is calculated. The notations u and y will be used, instead of $\tilde{u}$ and $\tilde{y}$.

It can be shown that

$$G_{\text{BLA}}(k) = \frac{S_{YU}(k)}{S_{UU}(k)}, \tag{8}$$

where the expectation in the cross-power and auto-power spectra is again taken with respect to the random input u. Note that for periodic excitations, (8) reduces to (Schoukens, Pintelon & Rolain, 2012)

$$G_{\text{BLA}}(k) = E_u\left\{\frac{Y(k)}{U(k)}\right\}. \tag{9}$$

It follows from (8) and Bussgang's theorem (Bussgang, 1952) that the BLA of the considered Wiener-Hammerstein system for Gaussian excitations is proportional to the product of the underlying dynamics. This is summarized in the following theorem.

Theorem 1. The BLA of the Wiener-Hammerstein system in (3), excited by Gaussian noise or by a random-phase multisine, is equal to

$$G_{\text{BLA}}(k) = c_{\text{BLA}} R(k) S(k) + O(N^{-1}), \tag{10}$$

where c_{BLA} is a constant that depends upon the odd nonlinearities in $f(x)$ and the power spectrum of the input signal.

Proof. This is shown in Pintelon & Schoukens (2012, pp. 85–86). □

The constant c_{BLA} is nonzero if $f(x)$ is non-even around the operating point. Theorem 1 shows that it is easy to measure the product $R(k)S(k)$ of a Wiener-Hammerstein system by measuring its BLA for an (asymptotically) Gaussian excitation.

3.3 The output spectrum of the BLA

An explicit expression for the output spectrum of the BLA of a Wiener-Hammerstein system, excited by a random-phase multisine, is derived in this subsection. For the more complex case of a phase-coupled multisine, a similar derivation will be used (see Theorem 2).

Under Assumptions (A1) and (A4), the noise-free output spectrum of the Wiener-Hammerstein system in (3) is equal to

$$Y(k) = \gamma_0 + \sum_{D=1}^{\infty} \gamma_D Y_D(k), \tag{11}$$

where $Y_D(k)$ is the noise-free output spectrum of a Wiener-Hammerstein system that contains a pure Dth-degree nonlinearity ($f(x) = x^D$). The multiplication in the time domain corresponds to a convolution in the frequency domain, and thus (also keeping in mind the normalization factor in the inverse DFT in (2))

$$Y_D(k) = \left(\frac{1}{\sqrt{N}}\right)^{D-1} S(k) \sum_{l_1,l_2,\ldots,l_D=-N/2+1}^{N/2} \prod_{i=1}^{D} R(l_i)U(l_i), \tag{12}$$

such that $\sum_{i=1}^{D} l_i = k$. The only terms in $Y_D(k)$ that contribute to the BLA are those where the product $\prod_{i=1}^{D} U(l_i)$ has a phase $\phi_k = \angle U(k)$. Terms that also depend on $\phi_{l\neq k}$ will be eliminated in the expected value $E_u\{Y(k)U^*(k)\}$ in (8) or in the expected value in (9). The contributing terms are those where one of the l_is is equal to k, and where the other factors combine pairwise to $X(l)X(-l) = |X(l)|^2$. Note that this is only possible if D is odd. Summing up all the terms in (12) that contribute to the BLA results in

$$Y_{D,\text{BLA}}(k) = D!S(k)R(k)U(k)\left(\frac{1}{N}\sum_{l=-N/2+1}^{N/2}|X(l)|^2\right)^{\frac{D-1}{2}} + O(N^{-1}). \tag{13}$$

For example, for $f(x) = x^3$, the BLA is equal to

$$G_{\text{BLA}}(k) = 6S(k)R(k)\left(\frac{1}{N}\sum_{l=-N/2+1}^{N/2}|X(l)|^2\right) + O(N^{-1}). \tag{14}$$

The error term $O(N^{-1})$ is due to the fact that there are six permutations of $(k, l, -l)$ if $k \neq l$, while there are only three permutations of $(k, k, -k)$.

4 The proposed method

In this section, we propose to use a special type of multisines, namely phase-coupled multisines. After defining phase-coupled multisines, it is shown how the use of these signals makes it possible to separate the input and the output dynamics. Finally, a practical issue when working with phase-coupled multisines is addressed.

4.1 Phase-coupled multisine excitation

Phase-coupled multisines are multisines where specifically selected pairs of frequency lines where excitation is present have the same phase. Depending on whether excitation is present at both even and odd, or only at odd frequency lines, we are dealing with a full or an odd phase-coupled multisine, respectively.

Definition 4 (full phase-coupled multisine)**.** A signal $u(t)$ is a phase-coupled multisine if it is a multisine (see Definition 1) where excitation is only present at frequency lines k for which

$$\pm k \in \left\{ \left(\frac{d}{2} + di, \frac{d}{2} + di + s \right) \right\} \quad \text{for } i = 0, 1, \ldots, i_{\max}\,, \tag{15}$$

where d and s are integers (more details below), and if each of the frequency couples gets assigned an independently and identically distributed random phase $\phi_{\frac{d}{2}+di} = \phi_{\frac{d}{2}+di+s}$ with the property $E\left\{e^{j\phi_{\frac{d}{2}+di}}\right\} = 0$. For a full phase-coupled multisine, the even integer $d \geq 4$ determines the frequency resolution (excitation is present only every dth frequency line, starting from the frequency lines $\frac{d}{2}$ and $\frac{d}{2}+s$), and $s = c_{\text{shift}}d + 1$ will determine the shift of the poles and the zeros of $R(q)$ with respect to those of $S(q)$, where $c_{\text{shift}} > 0$ is an integer.

It can be useful to only have excitation present at the odd frequency lines, just as with random-phase multisines (Schoukens, Pintelon, Dobrowiecki & Rolain, 2005). The definition of the phase-coupled multisine then slightly changes.

Definition 5 (odd phase-coupled multisine)**.** A signal $u(t)$ is an odd phase-coupled multisine if it is a phase-coupled multisine (see Definition 4) where $\frac{d}{2} \geq 5$ is an odd integer, and where $s = c_{\text{shift}}d + 2$.

To simplify the notation in the rest of the paper, define

$$m := \frac{d}{2} + di\,. \tag{16}$$

Remark 2. Although this is not really necessary, the requirement $d \geq 4$ for a full phase-coupled multisine, and $\frac{d}{2} \geq 5$ for an odd phase-coupled multisine makes sure that there is no excitation present at the frequency lines $k = m - s$ and $k = m + 2s$. Hence, the output spectrum at these frequency lines will not be disturbed by linear contributions.

4.2 New terms in the output spectrum of the BLA

Since $U(m)$ and $U(m+s)$ have the same phase in a phase-coupled multisine, also other terms than the ones reported in (13) will contribute to the BLA at the frequency lines m and $m+s$. Moreover, the output spectrum will contain terms that are proportional to $S(k)$ and shifted versions of $R(k)$ at some frequency lines where no excitation is present. This is explained below.

Let us take a look at the terms in $Y_D(k)$ in (12) where the product $\prod_{i=1}^{D} U(l_i)$ has a phase $\angle U(m)$. These are the terms where one of the frequency lines l_i is equal to m or $m+s$ ($U(m+s)$ has the same phase as $U(m)$), and where the remaining factors in the product $\left(\frac{1}{\sqrt{N}}\right)^{D-1} \prod_{i=1}^{D} R(l_i)U(l_i)$ combine pairwise to a constant. The possible values for these $\frac{D-1}{2}$ (complex) constants are either

$$c_0 = \frac{1}{N} \sum_{l=-N/2+1}^{N/2} X(l)X(-l)\,, \tag{17a}$$

$$c_{-s} = \frac{1}{N} \sum_{l=-N/2+1}^{N/2} X(l)X(-(l+s))\,, \tag{17b}$$

or

$$c_{s} = \frac{1}{N} \sum_{l=-N/2+1}^{N/2} X(-l)X(l+s)\,. \tag{17c}$$

Note that whenever a pair of factors combines to c_{-s}, a frequency shift $-s$ is introduced in the sum $\sum_{i=1}^{D} l_i = k$. Likewise, a frequency shift s is introduced whenever a pair of factors combines to $c_s = (c_{-s})^*$. There are thus $D+1$ frequency lines k that range from $m - \frac{D-1}{2}s$ to $m + \frac{D+1}{2}s$ in steps of s where the product $\prod_{i=1}^{D} U(l_i)$ has a phase $\angle U(m)$. The smallest frequency line ($k = m - \frac{D-1}{2}s$) is obtained when one frequency line l_i is equal to m, and when all the other frequency lines form pairs $(l, -(l+s))$. The largest frequency line ($k = m + \frac{D+1}{2}s$) is obtained when one frequency line l_i is equal to $m+s$, and when all the other frequency lines form pairs $(-l, l+s)$. From the discussion above, the following theorem follows:

Theorem 2. Under Assumptions (A1) and (A4), and for $i = -\frac{D-1}{2}, -\frac{D-1}{2}+1, \ldots, \frac{D+1}{2}$, the expectation $E_u\left\{\frac{Y_D(m+is)}{U(m)}\right\}$ is equal to

$$\begin{aligned} D!S(m+is) \Bigg[& R(m) \sum_{\sum_k s_k = is} \prod_{k=1}^{\frac{D-1}{2}} c_{s_k} \\ & + R(m+s)\frac{|U(m+s)|}{|U(m)|} \sum_{\sum_k s_k = (i-1)s} \prod_{k=1}^{\frac{D-1}{2}} c_{s_k} \Bigg] \\ & + O(N^{-1})\,, \end{aligned} \tag{18}$$

and $E_u\left\{\frac{Y_D(-(m+is))}{U(-m)}\right\} = \left(E_u\left\{\frac{Y_D(m+is)}{U(m)}\right\}\right)^*$ is equal to

$$D!S(-(m+is))\left[R(-m)\sum_{\sum_k s_k=-is}\prod_{k=1}^{\frac{D-1}{2}} c_{s_k} + R(-(m+s))\frac{|U(m+s)|}{|U(m)|}\sum_{\sum_k s_k=-(i-1)s}\prod_{k=1}^{\frac{D-1}{2}} c_{s_k}\right] + O(N^{-1}) \tag{19}$$

for the Wiener-Hammerstein system in (3), excited by a phase-coupled multisine (see Definitions 4 and 5), and where each $s_k \in \{-s, 0, s\}$.

Proof. The theorem follows immediately from the discussion above. □

From here on, the error term $O(N^{-1})$ will be dropped. For example, for $D = 3$, there are four frequency lines where $E_u\left\{\frac{Y_3(k)}{U(m)}\right\}$ has a nonzero mean. These are listed below.

(1) At frequency line $k = m - s$:

$$E_u\left\{\frac{Y_3(k)}{U(m)}\right\} = 6S(m-s)R(m)c_{-s} \tag{20a}$$

(2) At frequency line $k = m$:

$$E_u\left\{\frac{Y_3(k)}{U(m)}\right\} = 6S(m)R(m)c_0 + 6S(m)R(m+s)\frac{|U(m+s)|}{|U(m)|}c_{-s} \tag{20b}$$

(3) At frequency line $k = m + s$:

$$E_u\left\{\frac{Y_3(k)}{U(m)}\right\} = 6S(m+s)R(m+s)\frac{|U(m+s)|}{|U(m)|}c_0 + 6S(m+s)R(m)c_s \tag{20c}$$

(4) At frequency line $k = m + 2s$:

$$E_u\left\{\frac{Y_3(k)}{U(m)}\right\} = 6S(m+2s)R(m+s)\frac{|U(m+s)|}{|U(m)|}c_s \tag{20d}$$

The results at the frequency lines $k = m - s$ and $k = m + 2s$ are of particular interest. At these frequency lines, $E_u\left\{\frac{Y_3(k)}{U(m)}\right\}$ is proportional to $S(k)R(k+s)$ and $S(k)R(k-s)$, respectively. The frequency shift of the input dynamics R over a frequency $-s$ (or s) creates a shift of the poles and the zeros of R over a frequency $-s$ (or s). Note that the shifted poles and zeros are no longer real nor paired in complex conjugated couples. Hence, the rational transfer functions related to $E_u\left\{\frac{Y_3(m-s)}{U(m)}\right\}$ and $E_u\left\{\frac{Y_3(m+2s)}{U(m)}\right\}$ will have complex coefficients instead of real coefficients. This will be used in the next subsection.

4.3 The shifted BLA *and parametric smoothing*

For simplicity, we continue to explain the idea on a third-degree nonlinearity. The generalization to an arbitrary degree D is explained in Subsection 4.4. First, the FRF measurements $E_u\left\{\frac{Y_3(k)}{U(m)}\right\}$ and $E_u\left\{\frac{Y_3(k)}{U(-m)}\right\}$ will be collected at appropriate frequency lines k, such that only contributions are selected where the input and output dynamics shift over a unique frequency offset. Next, a parametric transfer function model will be identified to get direct access to the poles and the zeros of the system. As the shifted poles result in a transfer function model with complex coefficients, an adapted frequency domain estimator (Peeters, Pintelon, Schoukens & Rolain, 2001) will be used. Finally, the input and the output dynamics will be split by separating the shifting poles and zeros from those that do not move.

From (19), it follows that

$$E_u\left\{\frac{Y_3(-(m-s))}{U(-m)}\right\} = 6S(-(m-s))R(-m)c_s \tag{21}$$

and that

$$E_u\left\{\frac{Y_3(-(m+2s))}{U(-m)}\right\} = 6S(-(m+2s))R(-(m+s)) \times \frac{|U(m+s)|}{|U(m)|}c_{-s} \tag{22}$$

Hence, $E_u\left\{\frac{Y_3(k)}{U(-m)}\right\}$ is proportional to $S(k)R(k-s)$ at the frequency lines $k = -(m-s)$, while it is proportional to $S(k)R(k+s)$ at the frequency lines $k = -(m+2s)$. Therefore, by analogy with (9), define the shifted BLAs $G^+_{\text{SBLA}}(k)$ and $G^-_{\text{SBLA}}(k)$ by collecting $E_u\left\{\frac{Y(k)}{U(m)}\right\}$ and $E_u\left\{\frac{Y(k)}{U(-m)}\right\}$ at the appropriate frequency lines k, such that contributions proportional to $S(k)R(k+s)$ and $S(k)R(k-s)$, respectively, result:

Definition 6 (shifted best linear approximation)**.** For a system excited by a phase-coupled multisine (see Definitions 4 and 5), the shifted BLA $G^+_{\text{SBLA}}(k)$ is defined as

$$G^+_{\text{SBLA}}(k) := \begin{cases} E_u\left\{\frac{Y(k)}{U(m)}\right\} & \text{at } k = m - s \\ E_u\left\{\frac{Y(k)}{U(-m)}\right\} & \text{at } k = -(m+2s) \end{cases} \tag{23}$$

while the shifted BLA $G^-_{\text{SBLA}}(k)$ is defined as

$$G^-_{\text{SBLA}}(k) := \begin{cases} E_u\left\{\frac{Y(k)}{U(m)}\right\} & \text{at } k = m + 2s \\ E_u\left\{\frac{Y(k)}{U(-m)}\right\} & \text{at } k = -(m-s) \end{cases} \tag{24}$$

with m defined in (16).

Since $G^-_{\text{SBLA}}(k) = \left(G^+_{\text{SBLA}}(-k)\right)^*$, we can focus completely on one of both, e.g. $G^-_{\text{SBLA}}(k)$.

Next, a parametric transfer function model is identified on $G^-_{\text{SBLA}}(k)$, using a weighted least-squares estimator (Peeters et al., 2001)

$$\hat{\theta} = \arg\min_{\theta} K(\theta)\,, \tag{25a}$$

where the cost function $K(\theta)$ is equal to

$$\frac{1}{N} \sum_{k \in \{m+2s, -(m-s)\}} \frac{|G^-_{\text{SBLA}}(k) - G^-_{\text{SBLA}}(k,\theta)|^2}{\sigma^2_{G^-_{\text{SBLA}}}(k)}\,. \tag{25b}$$

Here, $G^-_{\text{SBLA}}(k,\theta)$ is a parametric transfer function model with the complex coefficients $b_{\text{SBLA,l}}$ and $a_{\text{SBLA,l}}$ collected in the parameter vector θ:

$$G^-_{\text{SBLA}}(k,\theta) = \frac{\sum_{l=0}^{n_R+n_S} b_{\text{SBLA},l} e^{-j2\pi\frac{k}{N}l}}{\sum_{l=0}^{m_R+m_S} a_{\text{SBLA},l} e^{-j2\pi\frac{k}{N}l}}\,, \tag{26}$$

and $\sigma^2_{G^-_{\text{SBLA}}}(k)$ is the sample variance of $G^-_{\text{SBLA}}(k)$. Since $G^-_{\text{SBLA}}(k)$ is proportional to $S(k)R(k-s)$, the poles (and the zeros) of R will be shifted over a frequency s, and will no longer be real, nor complex conjugated. By comparing the poles (and the zeros) of $G^-_{\text{SBLA}}(k,\theta)$ and their complex conjugates, the poles (and the zeros) of R and S can be separated. Indeed, a frequency shift $e^{j2\pi\frac{2s}{N}}$ will be visible in the complex plane between the shifted poles (and zeros) of R and their complex conjugates, while the poles (and zeros) of S will not show this shift. Fig. 2 shows an example of the pole shifting.

This approach has the potential to discriminate between a Wiener, a Hammerstein, and a Wiener-Hammerstein model, based on whether there are shifting poles/zeros (and thus input dynamics), fixed poles/zeros (and thus output dynamics), or both. A more detailed discussion on structure discrimination is provided in Schoukens, Pintelon, Rolain, Schoukens, Tiels, Vanbeylen, Van Mulders & Vandersteen (2015).

4.4 Generalization to an arbitrary degree D

The basic idea, that was explained for a cubic nonlinearity in the previous subsection, is now generalized to an arbitrary degree D. Under Assumption (A2), the result in Theorem 2 can be used to separate the input and the output dynamics. The main concern, however, is that the shifted BLAs will contain contributions where the input and the output dynamics are shifted over distinct frequencies if $D \geq 5$. This will be addressed now.

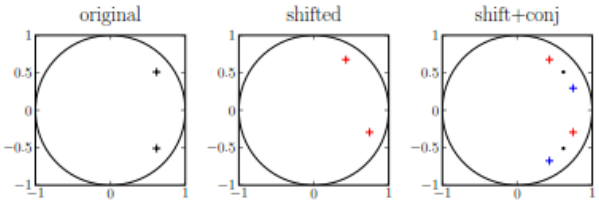

Fig. 2. Example of shifting poles (Left: original poles; Middle: shifted poles; Right: Shifted and conjugated poles).

The results in Theorem 2 show that the shifted BLA $G^-_{\text{SBLA}}(k)$ will not only contain terms that are proportional to $S(k)R(k-s)$ for $D \geq 5$, but also terms that are proportional to $S(k)R(k-2s)$. One way to deal with this is to redefine the shifted BLA, thereby only considering the outer frequency lines $k = m - \frac{D_{\max}-1}{2}s$ and $k = m + \frac{D_{\max}+1}{2}s$, where a unique frequency shift of R is present. The main disadvantage of this approach is that it requires knowledge of the maximal degree of nonlinearity $D_{\max}$. Moreover, in order not to be disturbed by linear contributions at these frequency lines, the frequency resolution of the phase-coupled multisine excitation should be lowered (cfr. Remark 2). Therefore, a different approach is followed here.

Both the contributions proportional to $S(k)R(k-s)$ and $S(k)R(k-2s)$ will make the poles of R shift over a positive frequency offset, while those of S will remain fixed. Hence, the poles and the zeros of R and S can still be separated. Since two distinct frequency shifts of the input dynamics are present in the shifted BLA, its parametric model should have a larger model order, namely the model order of S plus two times the model order of R. This will not be done, however, because the contributions that are proportional to $S(k)R(k-s)$ are dominant over those that are proportional to $S(k)R(k-2s)$ (see Appendix A), certainly if we assume that the cubic nonlinearities dominate the higher-order contributions. Hence, the terms in $G^-_{\text{SBLA}}(k)$ that are not proportional to $S(k)R(k-s)$ will simply be considered as nuisance terms.

4.5 Time origin

Since phase-coupled multisines rely on the fact that some frequency lines have equal phase, the time origin is important. This synchronization issue is addressed now.

Suppose that the input and the output measurements are shifted over a time δ, i.e. t becomes $t - \delta$. This results in a frequency-dependent phase shift in the input and the

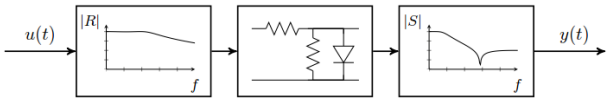

Fig. 3. The Wiener-Hammerstein benchmark system consists of a diode-resistor network sandwiched in between two third-order Chebyshev filters.

output spectrum. For example, $U(k)$ becomes $U(k)e^{jk\Delta}$, with $\Delta = -\frac{2\pi\delta}{N}$. Since the shifted BLA is defined as the expected value of the ratio of the input and the output spectrum at distinct frequency lines (see Definition 6), a phase shift is present in this shifted BLA:

$$E_u\left\{\frac{Y(k)}{U(m)}\right\} \to E_u\left\{\frac{Y(k)}{U(m)}e^{j(k-m)\Delta}\right\}. \qquad (27)$$

Since δ does not need to be an integer, the compensation for a shifted time origin will be done in the frequency domain. The phase shift Δ can be determined for each pair of frequency lines at which excitation is present as

$$\Delta(m) = \frac{\angle U(m+s) - \angle U(m)}{s}, \qquad (28)$$

and the expected values in the shifted BLAs can be compensated by multiplying $E_u\left\{\frac{Y(k)}{U(m)}\right\}$ with $e^{j(m-k)\Delta(m)}$, and $E_u\left\{\frac{Y(k)}{U(-m)}\right\}$ with $e^{j(-m-k)\Delta(m)}$.

5 Experimental results

This section illustrates the proposed method on experimental data obtained from the Wiener-Hammerstein benchmark system (Schoukens et al., 2009).

5.1 *Device*

The Wiener-Hammerstein benchmark system is an electronic circuit with a Wiener-Hammerstein structure. It consists of a diode-resistor network sandwiched in between two third-order filters (see Fig. 3). The input filter R is a Chebyshev low-pass filter with a ripple of 0.5 dB and a cut-off frequency of 4.4 kHz. The output filter S is an inverse Chebyshev filter with a stop-band attenuation of 40 dB starting at 5 kHz. It has a transmission zero in the frequency band of interest.

5.2 *Measurement data*

The benchmark data were obtained using a filtered Gaussian noise excitation (Schoukens et al., 2009) and are therefore not used in this paper. Here, a random-phase multisine is used to measure the BLA, and an odd phase-coupled multisine is used to measure the shifted BLA. For both excitations, the input and output are measured at a sample frequency of 78 125 Hz.

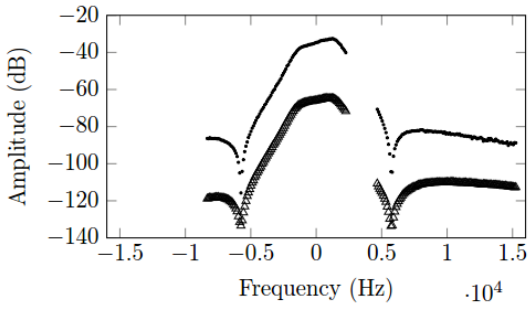

Fig. 4. The shifted BLA (black dots) is not symmetric around the origin. Its standard deviation is shown in black triangles.

The random-phase multisine contains $N = 8192$ samples. It has a flat amplitude spectrum with 682 frequencies ranging from 19 Hz to 13 800 Hz where excitation is present, and an rms level of 380 mV. This relatively small rms level is chosen to keep the nonlinear distortion level small. Seven phase realizations and three periods are applied. The first period is removed to avoid the effects of transients.

The phase-coupled multisine contains $N = 8192$ samples as well, and also has a flat amplitude spectrum. With $d = 10$, $s = 242$, and $i_{\max} = 111$, there are 224 frequencies that range from 47 Hz to 12 941 Hz where excitation is present. The signal is normalized to have a maximal amplitude of 2 V. This amplitude level corresponds more or less to that of the Wiener-Hammerstein benchmark data. Again, three periods are applied where the first one is removed to avoid the effects of transients. One thousand phase realizations are applied to almost completely average out the nonlinear distortions in the shifted BLA so that we can show a high-quality nonparametric estimate of the shifted BLA (see Fig. 4). However, much less phase realizations can be used, since the parametric modeling step will also reduce the impact of the nonlinear distortions (and the noise). For example, ten phase realizations can be enough (see Subsection 5.4).

5.3 *The* BLA *and the shifted* BLA

The BLA is first estimated non-parametrically via the robust method (Schoukens et al., 2012) using the random-phase multisine data. Next, a parametric fourth-order transfer function model is estimated on top of the non-parametric BLA by minimizing a weighted least-squares cost function that is similar to (25b), but with real parameters θ. Although a sixth-order model is expected (R and S are both third-order filters), a fourth-order model seems enough for the data at hand (see Fig. 5). The poles and the zeros of the parametric model are used as a reference to compare them with those of the shifted BLA.

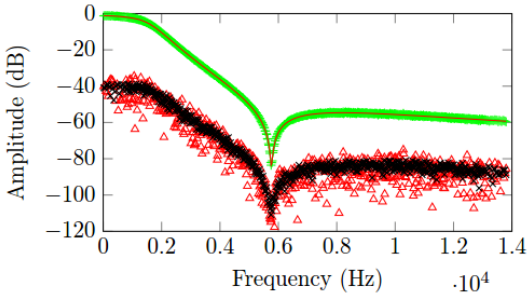

Fig. 5. A parametric fourth-order model (red line) can explain the non-parametric BLA (green) (the magnitude of the complex difference between the BLAs (red triangles) coincides with the estimated total distortion level (black)).

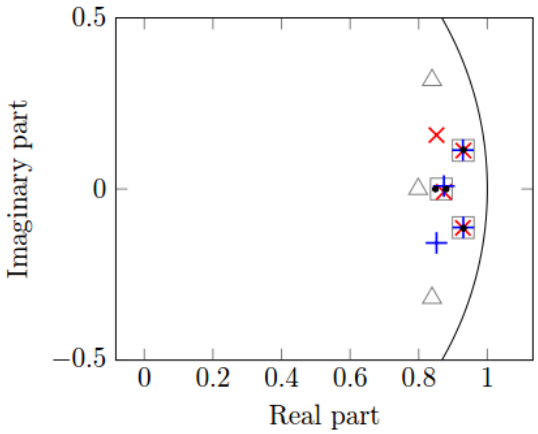

Fig. 6. The poles of the shifted BLA are shown in red crosses, their complex conjugates in blue pluses, and the original poles of the BLA in black dots. One pole (where red and blue are not on top of each other) shows a clear shift and can be assigned to the input filter R. The three other poles (almost) remain invariant and can be assigned to the output filter S. This is in good agreement with the internal structure of the filters in Fig. 3. Their poles are added in gray as a reference (triangles: R, squares: S).

The shifted BLA is estimated non-parametrically by averaging over the 1000 realizations of the input. The averaged value is shown together with its standard deviation in Fig. 4. Observe that the amplitude characteristic is not symmetric around the origin. Hence, a parametric transfer function model with complex coefficients is required. A fourth-order model is estimated using the weighted least-squares approach in (25). The poles of this model, together with their complex conjugates and the original poles of the BLA are shown in Fig. 6. A similar picture for the zeros is shown in Fig. 7.

5.4 Discussion of the results

One real pole can be assigned to the input filter R, since the corresponding pole of the shifted BLA shows a clear shift of about 21° with respect to its complex conjugate. This shift also nicely corresponds to the expected shift of

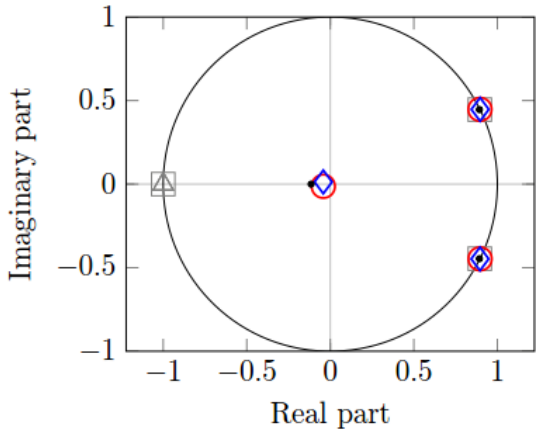

Fig. 7. Zeros of the shifted BLA are shown in red circles, their complex conjugates in blue diamonds, and zeros of the BLA in black dots. One zero outside the unit circle is not shown. The complex pair of zeros can clearly be assigned to the output filter S. The other zeros cannot be classified. The zeros of the filters in Fig. 3 are added in gray as a reference (triangles: R, squares: S).

$\frac{2s}{N}360° = 21.3°$. The other poles do (almost) not move. They can be assigned to the output filter S. Considering the internal structures of the filters (see Subsection 5.1), the poles are assigned correctly (see also Fig. 6). The input filter R should have a complex conjugate pole pair as well, but its effect on the FRFs seems unnoticeable due to the presence of the transmission zero in S (see also Subsection 5.3).

The complex pair of zeros can be assigned to the output filter S, since these zeros do not shift. This pair of zeros is assigned correctly, as it corresponds to the transmission zero in the output filter (see Subsection 5.1 and Fig. 7). The real zero in Fig. 7 cannot be clearly assigned. Although a shift of about 35° is present between the corresponding zero of the shifted BLA and its complex conjugate, its amplitude is so small that a small uncertainty on the zero position can completely change its classification. The inability to assign most of the zeros is to be expected, since, except for the transmission zero, the true zeros are at -1, and there is no excitation present in that part of the frequency band. Therefore, the uncertainty on these estimated zero positions is large, which prohibits their classification.

Similar results can be obtained when only ten phase realizations are used instead of one thousand. The 1000 experiments were split in 100 groups of ten phase realizations. In 61 cases, a correct assignment of the poles and zeros could clearly be made. In 36 of the remaining cases, the most damped real pole could have been wrongfully assigned to S, while the least damped real pole would then have been wrongfully assigned to R. The wrong assignment of these poles is likely to have a small impact on the further initialization of the Wiener-Hammerstein model, since both real poles lie close to each other. Only

in 3 cases, it was unclear whether both real poles should be assigned to R, to S, or one to R and one to S.

6 Conclusion

The best linear approximation (BLA) of a Wiener-Hammerstein system that is excited by Gaussian noise or a random-phase multisine is proportional to the product of the underlying linear dynamic blocks. By applying a more specialized phase-coupled multisine, it is shown that a modified BLA expression is proportional to the product of the output dynamics and a frequency-shifted version of the input dynamics. On the basis of the non-parametric measurement of this modified BLA, it is shown to be possible to assign the identified poles and zeros to either the input or output dynamics, provided that the poles and zeros are properly excited. This is confirmed by experimental results on the Wiener-Hammerstein benchmark system.

The proposed method has the potential to discriminate between a Wiener, a Hammerstein, and a Wiener-Hammerstein model, based on whether there are shifting poles/zeros (and thus input dynamics), fixed poles/zeros (and thus output dynamics), or both.

Future work is to derive variance expressions for the shifted BLA, from which bounds on the estimated shifted poles/zeros can be calculated. With these bounds, it will be possible to determine whether a pole/zero significantly shifted or not. This will enable an automatic assignment of the poles and the zeros.

Acknowledgements

The research leading to these results has received funding from the European Research Council under the European Union's Seventh Framework Programme (FP7/2007-2013)/ERC Grant Agreement n. 320378. This work was also supported in part by the Fund for Scientific Research (FWO-Vlaanderen), by the Flemish Government (Methusalem 1), and by the Belgian Federal Government (IAP DYSCO VII/19).

References

Bai, E.-W., Cai, Z., Dudley-Javorosk, S., & Shields, R. K. (2009). Identification of a modified Wiener-Hammerstein system and its application in electrically stimulated paralyzed skeletal muscle modeling. *Automatica*, *45*, 736–743.

Billings, S. A., & Fakhouri, S. Y. (1982). Identification of systems containing linear dynamic and static nonlinear elements. *Automatica*, *18*, 15–26.

Bussgang, J. J. (1952). *Crosscorrelation functions of amplitude-distorted Gaussian signals*. Technical Report 216. MIT research laboratory of electronics.

Chen, C. H., & Fassois, S. D. (1992). Maximum likelihood identification of stochastic Wiener-Hammerstein-type non-linear systems. *Mechanical Systems and Signal Processing*, *6*, 135–153.

Crama, P., & Schoukens, J. (2005). Computing an initial estimate of a Wiener-Hammerstein system with a random phase multisine excitation. *IEEE Transactions on Instrumentation and Measurement*, *54*, 117–122.

Dewhirst, O. P., Simpson, D. M., Angarita, N., Allen, R., & Newland, P. L. (2010). Wiener-Hammerstein parameter estimation using differential evolution - application to limb reflex dynamics. In *Third International Conference on Bio-inspired Systems and Signal Processing (BIOSIGNALS 2010), January 20–23, Valencia, Spain*.

Giri, F., & Bai, E.-W. (Eds.) (2010). *Block-oriented Nonlinear System Identification*. (1st ed.). Springer.

Isaksson, M., Wisell, D., & Rönnow, D. (2006). A comparative analysis of behavioral models for RF power amplifiers. *IEEE Transactions on Microwave Theory and Techniques*, *54*, 348–359.

Korenberg, M. J., & Hunter, I. W. (1986). The identification of nonlinear biological systems: LNL cascade models. *Biol. Cybern.*, *55*, 125–134.

Mu, B.-Q., & Chen, H.-F. (2014). Recursive identification of errors-in-variables Wiener-Hammerstein systems. *European Journal of Control*, *20*, 14–23.

Peeters, F., Pintelon, R., Schoukens, J., & Rolain, Y. (2001). Identification of rotor-bearing systems in the frequency domain. Part II: Estimation of modal parameters. *Mechanical Systems and Signal Processing*, *15*, 775–788.

Pintelon, R., & Schoukens, J. (2012). *System Identification: A Frequency Domain Approach*. (2nd ed.). Wiley-IEEE Press.

Schoukens, J., Pintelon, R., Dobrowiecki, T., & Rolain, Y. (2005). Identification of linear systems with nonlinear distortions. *Automatica*, *41*, 491–504.

Schoukens, J., Pintelon, R., & Rolain, Y. (2012). *Mastering System Identification in 100 Exercises*. Wiley-IEEE Press.

Schoukens, J., Pintelon, R., Rolain, Y., Schoukens, M., Tiels, K., Vanbeylen, L., Van Mulders, A., & Vandersteen, G. (2015). Structure discrimination in block-oriented models using linear approximations: a theoretic framework. *Automatica*, *53*, 225–234.

Schoukens, J., Suykens, J., & Ljung, L. (2009). Wiener-Hammerstein benchmark. In *15th IFAC Symposium on System Identification, July 6–8, St. Malo, France*.

Schoukens, J., Tiels, K., & Schoukens, M. (2014a). Generating initial estimates for Wiener-Hammerstein systems using phase coupled multisines. In *19th IFAC World Congress, August 24–29, Cape Town, South Africa*.

Schoukens, M., Pintelon, R., & Rolain, Y. (2014b). Identification of Wiener-Hammerstein systems by a nonparametric separation of the best linear approximation. *Automatica*, *50*, 628–634.

Sjöberg, J., Lauwers, L., & Schoukens, J. (2012). Iden-

tification of Wiener-Hammerstein models: Two algorithms based on the best split of a linear model applied to the SYSID'09 benchmark problem. *Control Engineering Practice*, *20*, 1119–1125.

Sjöberg, J., & Schoukens, J. (2012). Initializing Wiener-Hammerstein models based on partitioning of the best linear approximation. *Automatica*, *48*, 353–359.

Vandersteen, G., Rolain, Y., & Schoukens, J. (1997). Non-parametric estimation of the frequency-response functions of the linear blocks of a Wiener-Hammerstein model. *Automatica*, *33*, 1351–1355.

Weiss, M., Evans, C., & Rees, D. (1998). Identification of nonlinear cascade systems using paired multisine signals. *IEEE Transactions on Instrumentation and Measurement*, *47*, 332–336.

Weisstein, E. W. (n.d.). Weierstrass approximation theorem. From MathWorld—A Wolfram Web Resource. http://mathworld.wolfram.com/WeierstrassApproximationTheorem.html. Last visited on 3/4/2015.

Westwick, D. T., & Schoukens, J. (2012). Initial estimates of the linear subsystems of Wiener-Hammerstein models. *Automatica*, *48*, 2931–2936.

Wills, A., & Ninness, B. (2012). Generalised Hammerstein-Wiener system estimation and a benchmark application. *Control Engineering Practice*, *20*, 1097–1108.

A Dominant terms in the shifted BLA

The contributions in $G^{-}_{\mathrm{SBLA}}(k)$ that are proportional to $S(k)R(k-s)$ are dominant over those that are proportional to $S(k)R(k-2s)$. This is shown in this appendix.

First, it will be shown that $c_0 > |c_s|$. We have that

$$c_0 = \frac{2}{N}\sum_m |X(m)|^2 + |X(m+s)|^2\,, \tag{A.1}$$

and that

$$\begin{aligned} |c_s| &= \frac{2}{N}\left|\sum_m X(-m)X(m+s)\right| \\ &\leq \frac{2}{N}\sum_m |X(-m)X(m+s)|\,. \end{aligned} \tag{A.2}$$

By working out $(|X(m)| - |X(m+s)|)^2$ and rearranging the terms, we have

$$\begin{aligned} &|X(m)|^2 + |X(m+s)|^2 \\ &\quad = 2|X(m)||X(m+s)| + (|X(m)| - |X(m+s)|)^2\,, \end{aligned} \tag{A.3}$$

and thus $c_0 \geq 2|c_s|$.

Let $\alpha_D(k)$ be the ratio of the contributions in $Y_D(k)$ that are proportional to $S(k)R(k-s)$ and those that are proportional to $S(k)R(k-2s)$. Then we need to show that $|\alpha_D(k)| > 1$. From Theorem 2, we have

$$\alpha_D(k) = \frac{\frac{|U(m+s)|}{|U(m)|}\sum\limits_{\sum_k s_k = s}\prod\limits_{k=1}^{\frac{D-1}{2}} c_{s_k}}{\sum\limits_{\sum_k s_k = 2s}\prod\limits_{k=1}^{\frac{D-1}{2}} c_{s_k}} \tag{A.4}$$

at the frequency lines $k = m + 2s$, and

$$\alpha_D(k) = \frac{\sum\limits_{\sum_k s_k = s}\prod\limits_{k=1}^{\frac{D-1}{2}} c_{s_k}}{\frac{|U(m+s)|}{|U(m)|}\sum\limits_{\sum_k s_k = 2s}\prod\limits_{k=1}^{\frac{D-1}{2}} c_{s_k}} \tag{A.5}$$

at the frequency lines $k = -(m-s)$. As a factor $\frac{|U(m+s)|}{|U(m)|} > 1$ would be advantageous in one case, and disadvantageous in the other case, simply consider $\frac{|U(m+s)|}{|U(m)|} = 1$. Since the s_ks in the numerator should sum up to s, at least one factor c_s should be present in the numerator. Likewise, two factors c_s should be present in the denominator. The remaining s_ks should sum up to zero. Hence,

$$\alpha_D(k) = \frac{c_s}{c_s c_s}\frac{\sum\limits_{\sum_k s_k = 0}\prod\limits_{k=1}^{\frac{D-3}{2}} c_{s_k}}{\sum\limits_{\sum_k s_k = 0}\prod\limits_{k=1}^{\frac{D-5}{2}} c_{s_k}}\,. \tag{A.6}$$

A zero-sum of the s_ks is possible if all of them are zero. Furthermore, one or more pairs $c_0 c_0$ can be replaced by $c_s c_{-s} = |c_s|^2$. Hence,

$$\begin{aligned} |\alpha_D(k)| &= \frac{1}{|c_s|}\frac{\sum\limits_{i=0}^{\lfloor\frac{D-3}{4}\rfloor} c_0^{\frac{D-3}{2}-2i}|c_s|^{2i}}{\sum\limits_{i=0}^{\lfloor\frac{D-5}{4}\rfloor} c_0^{\frac{D-5}{2}-2i}|c_s|^{2i}} \\ &\geq \frac{c_0}{|c_s|}\,, \end{aligned} \tag{A.7}$$

and since $c_0 \geq 2|c_s|$, we have $|\alpha_D(k)| \geq 2 > 1$. For $D = 3$, there are no contributions proportional to $S(k)R(k-2s)$, so that $\alpha_3(k) \to \infty$.